Physica Status Solidi A: Applications and Materials Science

Potential of epitaxial silicon carbide microbeam resonators for chemical sensing

--Manuscript Draft--

Manuscript Number:	pssa.201600437R1
Full Title:	Potential of epitaxial silicon carbide microbeam resonators for chemical sensing
Article Type:	Original Paper
Section/Category:	Wide bandgap semiconductors for electron devices - E-MRS Spring 2016 Symp L
Keywords:	3C-SiC; residual stress; MEMS; resonant sensing; Q factors
Corresponding Author:	Francesca Iacopi, PhD Griffith University Nathan, Queensland AUSTRALIA
Corresponding Author Secondary Information:	
Corresponding Author's Institution:	Griffith University
Corresponding Author's Secondary Institution:	
First Author:	Atieh R Kermany
First Author Secondary Information:	
Order of Authors:	Atieh R Kermany
	James S Bennett
	Victor M Valenzuela
	Warwick P Bowen
	Francesca Iacopi, PhD
Order of Authors Secondary Information:	
Abstract:	Epitaxial silicon carbide is promising for chemical resonant sensing applications due to its excellent mechanical, thermal, and biochemical properties. This paper reviews six important aspects of (1) silicon carbide heteroepitaxial growth and residual stress; (2) silicon carbide beam resonators, resonator types, and fabrication processes; (3) sensing principles, dynamic sensing mechanical performance and transduction techniques; (4) damping parameters; (5) mean stress influence on mass sensitivity of SiC flexural microbridge resonators; and (6) gradient stress impact on SiC cantilever static behavior. The primary goal is to suggest the means to improve the mass sensitivity parameter and application range of epitaxial silicon carbide microbeam resonators and benchmark it with other relevant materials.
Additional Information:	
Question	**Response**
Please submit a plain text version of your cover letter here. Please note, if you are submitting a revision of your manuscript, there is an opportunity for you to provide your responses to the reviewers later; please do not add them to the cover letter.	Dear Editors, We would like to thank you as well as the reviewers for considering our manuscript with title "Stress management and potential of epitaxial silicon carbide microbeam resonators for chemical sensing" for publication in Physica Status Solidi A, special issue for the Wide bandgap semiconductors for electron devices - E-MRS Spring 2016 Symposium L. We are now ready to submit our revised version, which takes into account the reviewers' comments and where we have highlighted all changes in yellow. We attach also a point-by-point response document. Yours sincerely,

Powered by Editorial Manager® and ProduXion Manager® from Aries Systems Corporation

	Francesca Iacopi

Powered by Editorial Manager® and ProduXion Manager® from Aries Systems Corporation

Revised Manuscript

Review copy – not for distribution

(pss-logo will be inserted here by the publisher)

Potential of epitaxial silicon carbide microbeam resonators for chemical sensing

Atieh R. Kermany[1], James S. Bennett[2], Victor M. Valenzuela[2,3], Warwick P. Bowen[2] and Francesca Iacopi[*,1]

[1] Environmental Futures Research Institute, Griffith University, Nathan, 4111 QLD, Australia
[2] School of Mathematics and Physics, The University of Queensland, QLD 4072, Australia
[3] Facultad de Ciencias Físico-Matemáticas, Universidad Autónoma de Sinaloa, SIN 80000, México

Received ZZZ, revised ZZZ, accepted ZZZ
Published online ZZZ(Dates will be provided by the publisher.)

Keywords: Epitaxial silicon carbide, microbeam resonator, dynamic sensing, residual stress

* Corresponding author: e-mail f.iacopi@griffith.edu.au, Phone: tel +61 7 373 58014

Epitaxial silicon carbide is promising for chemical resonant sensing applications due to its excellent mechanical, thermal, and biochemical properties. This paper reviews six important aspects of (1) silicon carbide heteroepitaxial growth and residual stress; (2) silicon carbide beam resonators, resonator types, and fabrication processes; (3) sensing principles, dynamic sensing mechanical performance and transduction techniques; (4) damping parameters; (5) mean stress influence on mass sensitivity of SiC flexural microbridge resonators; and (6) gradient stress impact on SiC cantilever static behavior. The primary goal is to suggest the means to improve the mass sensitivity parameter and application range of epitaxial silicon carbide microbeam resonators and benchmark it with other relevant materials.

Copyright line will be provided by the publisher

1 Introduction Silicon carbide (SiC) has outstanding mechanical, biochemical, thermal, and electrical properties, making it a promising wide bandgap semiconductor material for sensing applications in harsh environments such as high temperature, vibration, and corrosive media, and when silicon (Si) has limitation [1-5]. SiC has many polytypes with different stacking sequences. The most common polytypes are hexagonal (2H, 4H and 6H-SiC), rhombohedral (15R and 21R-SiC) and cubic (3C-SiC). Among them, 3C-SiC is the only thermodynamically stable polytype that can be grown on a Si substrate heteroepitaxially and thus it is widely used for microelectromechanical systems (MEMS) applications, where it offers easy to micromachine, larger area, and lower cost production as compared with the bulk SiC substrates [6-8].

The first MEMS system, a gold microcantilever on a Si substrate (resonant gate transistor), was reported in 1967 [9]. Soon after that, Newell [10] reported the benefits of integrating micromechanical structures with electronic circuits through microfabrication techniques. Later, the invention of atomic force microscopy [11] in 1986 and the advancement in silicon surface and bulk micromachining processing capabilities made MEMS commercialization possible. Currently, MEMS technology plays an important role in many applications ranging from sensing, energy harvesting, and signal processing, to scanning probe microscopy and precision measurements in several fields of science and engineering [12]. The limitation of silicon for harsh environment applications has created the need for the application of the wide bandgap materials such as SiC. The integration of these new materials makes them excellent candidates as sensors, actuators, RF, and optical devices [2-4]. In particular, microresonators, which began to emerge in 1980s, are of interest due to their low mass and very high transduction sensitivity, resolution, and selectivity as the result of their quasi-digital frequency output signal [13, 14].

The aim of this paper is to present an overview on the enhancement of the mass sensitivity and application range of epitaxial SiC flexural microbeam resonators. The review includes: (1) heteroepitaxy of 3C-SiC on Si and residual stress; (2) silicon carbide beam resonators, resonator types, and fabrication processes; (3) sensing principles and transduction techniques; (4) dynamic sensing parameters (frequency (*f*) and quality factor (*Q*)); (5) damping parameters; (6) the influence of mean stress on mass sensitivity of SiC

Copyright line will be provided by the publisher

1
2
3
4
5
6
7
8
9
10
11
12
13
14
15
16
17
18
19
20
21
22
23
24
25
26
27
28
29
30
31
32
33
34
35
36
37
38
39
40
41
42
43
44
45
46
47
48
49
50
51
52
53
54
55
56
57
58
59
60
61
62
63
64
65

Table 1 Material properties of wide bandgap semiconductors applied in MEMS [2, 3, 12, 32-40].

Material	Si(100)	SiC(100)	SiC(111)	SiO_2	αSiN	GaN	GaAs	Diamond
Structure	cubic	cubic	Cubic	amorphous	amorphous	Wurzite	cubic	cubic
E_g (eV)	1.12	2.4	2.4	9	5	3.4	1.43	5.5
Lattice *a* (Å)	5.43	4.36	4.36	-	-	3.2	5.65	3.57
Lattice *c* (Å)	-	-	-	-	-	5.2	-	-
E (Gpa)	130	330	400	70	250	330	85	1220
ρ (kg/m^3)	2300	3200	3200	2200	3200	6100	5300	3500
ν	0.28	0.267	0.235	0.17	0.27	0.2	0.31	0.2
α (10^{-6}/K)	2.6	3	3	0.5	3	5.5	5.73	1
κ (W/m.K)	150	70	70	1	8	130	55	2000
T_m (K)	1690	3103	3103	1970	2170	2400	1510	4270
c_v (10^6J/m^{3}K)	1.6	3	3	1.5	3	3	3.5	1.8
Mohs Hardness	6-7	9-9.5	9-9.5	6-7	8.5	-	4-5	10

flexural microbridge resonators; (7) the impact of gradient stress on the static behavior of SiC cantilevers; and (8) further applications.

2 Heteroepitaxy of 3C-SiC on Si Epitaxial growth of SiC is performed through different techniques such as chemical vapour deposition (CVD) [15, 16], liquid phase epitaxy [17], and molecular beam epitaxy [18]. CVD is the most commonly used growth method and involves three general steps: (1) hydrogen surface etching to remove any native oxide; (2) a carbonization process to form a buffer (sealing) layer; and (3) the supply of gases to grow the 3C-SiC layer [19]. CVD growth parameters such as temperature, deposition rate, and pressure greatly impact the quality of the as-grown 3C-SiC films [20]. Modification of these parameters and the growth steps have led to the production of very high quality monocrystalline films [21].

Despite that, formation of defects such as misfit dislocation and stacking faults within the SiC crystal is inevitable due to the thermal expansion coefficients (~8%; during the cool down) and lattice constants (~20%) difference of Si and 3C-SiC [7, 22-24].

The large misfits between Si and SiC further generate residual stress within the SiC film. Residual stress includes mean stress (σ) and gradient stress. Both values are calculated from the stress profile $\sigma(z)$ across the SiC film, where z is the direction perpendicular to the film surface. Gradient stress ($\Delta\sigma$) is defined as $\sigma(z = t)$ - $\sigma(z = 0)$ and mean stress as $\sigma(z)$ or mean value across the film thickness [7, 25]. Many literature reports have focused on understanding the residual stress behavior, as the impact of the mean stress could be beneficial or disadvantageous depending on the application [26-29]. The residual stress further influences both static and dynamic performances of single-clamped and double-clamped resonators, as will be discussed in sections 7 and 8 (respectively).

2.1 Interface challenge One outstanding challenge of the epitaxial growth of SiC on Si is that the SiC-Si interface is unstable at high temperatures, and may result in the electrical shorting of the SiC film with the Si substrate. This can happen either upon film growth or during subsequent high temperature processing [30]. Therefore, a barrier stronger than the typical carbonization layer at the interface is required to avoid such interface failure [31].

3 Epitaxial SiC as beam resonator Many wide bandgap materials–including silicon carbide (SiC), silicon oxide (SiO_2), silicon nitride (αSiN), gallium nitride (GaN), gallium arsenide (GaAs), and diamond–-have been investigated for beam resonator fabrication, based on application and due to their excellent mechanical properties and chemical stability. Their properties including structure, bandgap (E_g), lattice constant (*lattice a* and *lattice c*), Young modulus (*E*), density (ρ), Poisson's ratio (ν), thermal expansion coefficient (α), thermal conductivity (κ), melting/ sublimation temperature (T_m), specific heat capacity per unit volume (c_v), and hardness (Mohs hardness) are shown in Table 1 [2, 3, 12, 32-40].

Provided the challenge in 2.1 is addressed, epitaxial SiC is potentially of choice for high temperature, high frequency, and harsh environment MEMS applications because of its high Young modulus to density ratio, hardness (due to its large Si-C bonding), and thermal conductivity. It also has high electrical stability, high resistance to radiation, and is biocompatible [2, 8, 41-43]. Although diamond nominally has superior material properties to epitaxial SiC, these are not accessible in single-crystalline epitaxial films. Additionally, diamond's fabrication is expensive and complex [44, 45].

3.1 Resonator types and modes of vibration Microresonator structures are broadly divided into ---beams and diaphragms--- where each group includes different shapes and clamping arrangements. Beam resonators can appear in different shapes, including single-clamped (s-c) or cantilever and double-clamped (d-c) or bridge as shown in Fig. 1 [14]. Long and narrow bridges are known as string resonators in literature.

Copyright line will be provided by the publisher

Resonators are further investigated according to their mechanical static or dynamic behaviour as will be discussed in section 4. Each resonator structure has multiple vibrational modes where each mode has its specific displacement pattern, frequency, and Q-factor. The vibration displacement pattern is further categorized into three forms; flexural (out-of-plane up and down movements and in-plane right and left movements); torsional (angular vibration along the rotation axis); and longitudinal (in-plane horizontal movements). The out-of-plane flexural mode is the most analysed variety. Each vibrational mode is named and numbered according to its vibration pattern and number of antinodes respectively [14]. Thus, all the modes have different frequencies and mode shapes. The first mode, which has the lowest frequency, is the fundamental, and the multiples of that frequency are called its harmonic overtones, as shown in Fig. 1 [46].

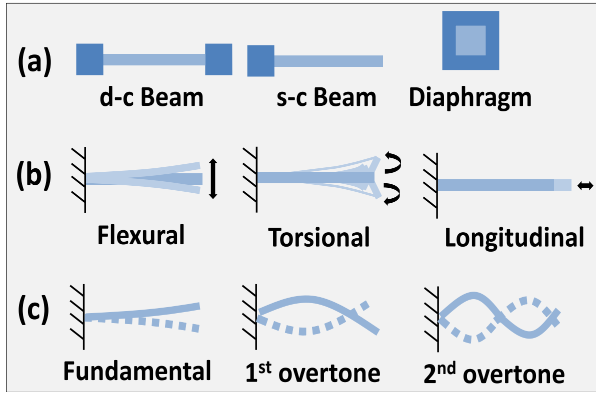

Figure 1 Schematic of (a) resonator types; anchors and resonators are shown in dark and light blue colours respectively, (b) vibration displacement patterns, and (c) first three modes of dynamic flexural vibration of a cantilever.

3.1.1 Beam theories Beam bending mechanisms are classified into two models, Timoshenko (TBT) and Euler Bernoulli (EBBT) [47]. Timoshenko beam theory was developed by Stephen Timoshenko in the early 20th century. The model includes both the shear contribution as the result of rotational inertia effects and the bending contribution of the beam deformation (Eq. (1)). This model is mostly suitable for short beams when the length (L) approaches the thickness (t) [48, 49]. The Timoshenko beam theory is simplified to the Euler Bernoulli beam theory for long beams (L/t > 25), when the rotational inertia effects can be neglected and the beam becomes rigid in shear. Euler Bernoulli beam theory helps in calculating and analyzing the lateral deflection of the beams as a function of only the bending contribution [50].

$$d_{TBT} = -\underbrace{\frac{FL}{\kappa GA}}_{Shear} - \underbrace{\frac{FL^3}{3EI}}_{Bending}, \qquad (1)$$

where d_{TBT} is the maximum vertical deflection, A is the cross section area ($A = wt$ for a rectangular shape; w is the width of a rectangular beam), κ is the shear coefficient (κ = 5/6 for a rectangular shape), F is the force, G is the shear modulus of the beam material, and I is the area moment of inertia ($I = wt^3/12$, for a rectangular beam). If the width of the beam is large compared to its thickness, such that $w \geq 5t$, it is necessary to replace E with $E\left(1-\nu^2\right)^{-1}$.

3.2 3C-SiC beam resonators fabrication process SiC on Si beam resonators can be fabricated using Si surface micromachining through four stages of: (1) photolithography; (2) SiC anisotropic etching; (3) Si isotropic etching; and (4) photoresist removal. Resonators fabricated in this manner have suspended and floating anchors as the result the isotropic etching (Fig. 3(a)). To overcome this and create perfect-clamped resonators, two photolithography steps can be used, as we reported in our earlier work [6]. The first lithography step is used to pattern the microresonator structures on the surface of the SiC film and the second step (Fig. 2) is used to cover the anchors prior to the isotropic Si etching in order to prevent them from being overetched. This is a much faster and easier approach than the backside bulk micromachining method previously reported in the literature [51]. The scanning electron microscopy (SEM) images in Fig. 3 show a comparison between perfect-clamped beams and beam resonators with suspended anchors.

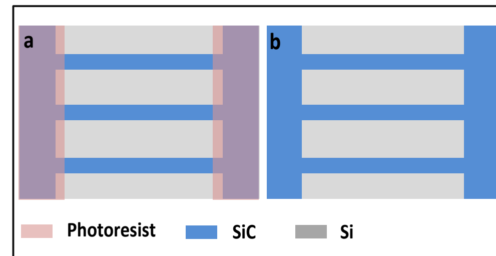

Figure 2 Top view schematic of perfect-clamped second photolithography step (a) second mask patterning (rectangle shapes covering the anchors) prior to the Si isotropic etching to protect the anchors and (b) perfect-clamped resonators after the Si etching and photoresist removal.

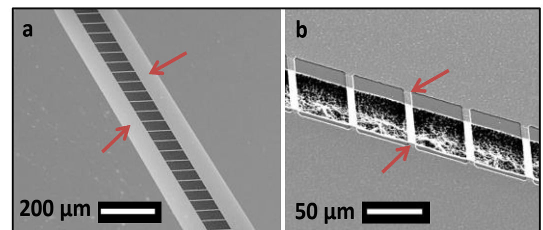

Figure 3 SEM images of (a) bridge resonators with suspended anchors and (b) perfect-clamped bridge resonators. The red arrows show (a) the suspended anchors, where the bridge resonators are all connected as the result of the SiC being

Copyright line will be provided by the publisher

1
2
3
4
5
6
7
8
9
10
11
12
13
14
15
16
17
18
19
20
21
22
23
24
25
26
27
28
29
30
31
32
33
34
35
36
37
38
39
40
41
42
43
44
45
46
47
48
49
50
51
52
53
54
55
56
57
58
59
60
61
62
63
64
65

overetched and (b) the protected anchors as the result of the second lithography step.

4 Sensing principles A beam with actuation and readout arrangements can work as a sensor [14]. In general, resonant sensors work by measuring the changes of resonator deflection (static response), or resonator frequency (dynamic response).

4.1 Static Response Adsorption of molecules on the resonator surface changes the surface free energy, surface energy density, or surface tension, thus causing different surface stresses on the two faces of the resonator when adsorption is restricted to one face of the oscillator. The molecule absorption further results in the deflection of the resonators such as cantilever as the result of the added mass [52-55]. Stoney's equation relates the differential surface stress (Δg) to the cantilever deflection (Δd) [56]:

$$\Delta d = \frac{4(1-\nu)}{E}\frac{L^2}{t^2}\Delta g. \quad (2)$$

It can be seen from Eq. (2) that the cantilever deflection increases by increasing the length and decreasing the thickness. The deflection could be downwards or upwards depending on the differential surface stress. A compressive differential stress results in a downwards bending whereas a tensile differential stress makes the bending upwards. The sensitivity of this detection mode has greatly increased and currently, surface stress changes of below 10^{-6} Nm^{-1} can be measured [32].

The final deflection in the cantilever is also affected by the cantilever intrinsic bending as the result of the gradient stress within the material, which is the case for the epitaxial SiC cantilevers as explained in section 2 [28, 57, 58]. This intrinsic bending reduces the application range of epitaxial SiC cantilevers for MEMS sensing applications and when flat structures are required. Therefore, it is important to understand and engineer the intrinsic bending in the cantilever to increase its application range. This is discussed in details in section 8.

The surface stress Δg is further related to factors such as electrostatic, steric, and hydrophobic interactions between the molecules on the cantilever surface [59-62], and the configurational entropy (including the buffer solution, if any), and the temperature variation [63-66].

The above considerations are only applicable to thin film cantilevers made of one material. Bimorph cantilevers consist of two materials with different material properties. For example, mismatched hygroscopicity causes deflection in response to humidity variations [67]. One common situation is thermal expansion mismatch [68], which can cause the cantilever to deflect in response to temperature changes according to [69]

$$\Delta d = \frac{3L^2(\alpha_1-\alpha_2)(\Delta T)}{h_2^2}\cdot N, \quad (3)$$

$$N = \left[\frac{(h_1+h_2)}{3(1+\frac{h_1}{h_2})^2 + (1+\frac{E_1h_1}{E_2h_2}) + (\frac{h_1}{h_2}+\frac{E_2h_2}{E_1h_1})}\right],$$

where E_1, E_2, h_1, h_2, α_1, and α_2 are the materials' Young modulus, thickness, and thermal expansion coefficients and ΔT is the temperature variation. Bimorph cantilevers can be used as thermal [68], humidity [67], or chemical [70] sensors.

4.2 Dynamic Response In the dynamic mode, the frequency of the resonator changes as the result of the added mass and the change in stiffness of the resonator upon molecular adsorption on its surface [32, 71]. The resonant frequency shift is dominated by the added mass when the molecules are adsorbed at the high vibrational amplitude points, while adsorption at nodal or clamping points predominately alters the stiffness [72]. Thus, it is important to control the position of the molecular adsorption through a surface functionalization process.

Generally, the resonator natural frequency reduces as the resonator mass increases [73, 74]. An explicit relationship which shows this can be simply established under the approximation that the stiffness, and therefore spring constant k_n of the resonator vibrational mode *n,* is unchanged by the added mass. This approximation is appropriate when the molecules adsorb at or near the points of high vibrational amplitude on the resonator. The resonance frequency shift (Δf_n) can then be straightforwardly determined using the relationship $k_n = m_{eff} f_n^2$ between the spring constant, effective mass (m_{eff}) and frequency of the resonator mode (f_n). In the case where the fractional change in the effective mass ($\Delta m_n/m_{eff}$) is small, it is straightforward to show that:

$$\frac{\Delta f_n}{f_n} = -\frac{\Delta m_n}{2m_{eff}}, \quad (4)$$

where it is natural to define the *mass sensitivity* $S_m = \Delta f_n/\Delta m_n = f_n/2m_{eff}$ [3].

We note, here, that the effective mass m_{eff} of a resonator mode is a fraction of the total mass m_{tot}, determined by the mode shape. For instance, for a bridge resonator:

$$m_{eff} = 0.735 m_{tot} = 0.735 Ltw\rho, \quad (5)$$

where the constant value of 0.735 represents the decreased contribution of mass near the clamping points [75-77]. Similarly, the change in effective mass Δm_n is a fraction of the total particle mass, depending on where the mass is added to the resonator. The change in effective mass only

Copyright line will be provided by the publisher

equals the total added mass if the mass is added at the position of peak amplitude of vibration.

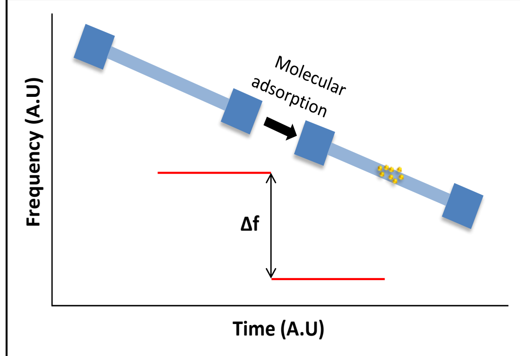

Figure 4 Schematic of a mass detection mechanism of a bridge.

4.2.1 Minimum resolvable mass

As discussed above, mass sensing is a common use of beam microresonators (Fig. 4), where the sensing is performed by measuring the frequency shift following adsorption [78, 79]. The uncertainty in this frequency shift measurement determines the resolution of the sensor. Two common strategies are used to perform precise measurements of the resonance frequency of micromechanical resonators.

In the first technique, the motion of the resonator is detected, delayed, amplified and fed-back onto the resonator via an applied force [80]. With correct choice of the delay, the applied force reinforces the velocity of the resonator providing a gain process that competes with its intrinsic damping. With sufficient amplification, this results in regenerative oscillation of the motion of the resonator, closely analogous to laser oscillation. The oscillation occurs at the mechanical resonance frequency, thereby allowing its precise determination.

In the second technique, the motion of the resonator is driven via an oscillatory force. The response to the force is maximised at the mechanical resonance frequency, or more generally, at each mechanical resonance frequency of the device. The phase of the response to the force varies linearly across the mechanical resonance. Tracking this phase within a phase-locked loop provides an accurate method to characterise the mechanical resonance frequency [80].

The above techniques have the same fundamental noise floor, which is determined by the thermally driven motion of the resonator. This noise floor results in a minimum detectable mass, or *mass resolution*, well approximated by [81]:

$$\delta m_n \approx 2m_{eff}\left(\frac{E_{th}}{E_{osc}}\right)^{1/2}\left(\frac{1}{Qf_n\tau}\right)^{1/2}, \qquad (6)$$

where $E_{th}=k_BT$ is the thermal energy of the resonator, with k_B and T Boltzmann's constant and the temperature, respectively, E_{osc} is the energy of the coherent oscillation of the resonator mode, and τ is the total measurement duration. It is clear from Eq. (6) that the mass resolution can be improved both by reducing the effective mass of the resonator and by increasing its $Q\times f_n$ product. However, reducing the size of a resonator both reduces the total adsorption area, and generally results in a decreased Q [82-84]. Therefore it is useful to consider two figures of merit to evaluate the sensor performance; $Q\times f_n$ (Hz) and $Q\times R$ (nm^{-1}), where R is the resonator's surface-to-volume ratio [77, 85-87].

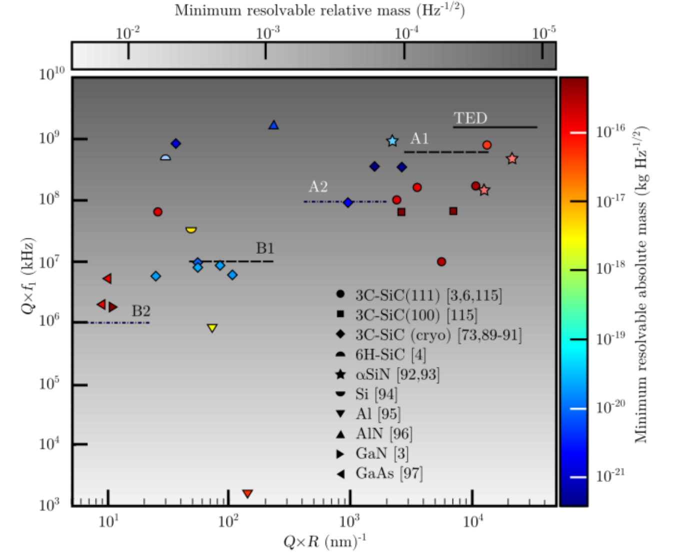

Figure 5 Literature survey of doubly-clamped beam resonators. Each point in the $Q\times R$–$Q\times f_1$ plane is experimental data. The table includes resonators of 3C-SiC(111) [3, 6, 88], 3C-SiC(100) [88], 3C-SiC (cryo) [73, 89-91], 6H-SiC [4], αSiN [92, 93], Si [94], Al (aluminium) [95], AlN (aluminium nitride) [96], GaN [3], and GaAs [97]. Points are coloured (right hand colour bar) according to the (theoretical) minimum resolvable mass (within a measurement time of one second), assuming that the device is operated under conditions of regenerative oscillation (Eq. (6)) with E_{osc}/E_{th}=~10^3. The upper colour bar corresponds to the background greyscale gradient; the minimum detectable mass as a fraction of the mode mass. The lines TED, A1, A2, B1 and B2 are theoretical calculations of the properties of 3C-SiC resonators for different lengths, widths and substrate thicknesses. We have included thermoelastic dissipation and clamping loss. Each line corresponds to sweeping the beam length from 200 μm (left end) to 1000 μm (right end). TED = thermoelastic dissipation limit, which is approximately independent of width; A = substrate thickness 25 μm, B = substrate thickness 2.5 μm; 1 = 4 μm width, 2 = 40 μm width. The beam thickness is fixed at 250 nm.

Figure 5 shows a survey of values of these figures of merit drawn from the literature on double-clamped beams. Every device represented was operated in vacuum conditions, such that medium damping is negligble. It is clear that the upper right corner, being the region of high $Q\times R$ and $Q\times f_1$, is dominated by large (~mm length scale) SiC and SiN bridges. Cryogenic devices, such as the AlN bridge [96], can enjoy higher absolute mass resolution due

Copyright line will be provided by the publisher

1
2
3 to their much smaller mass, but with the added
4 complication of integrating vacuum and cryogenic
5 conditions.
6 We also show theoretical limits on the figures of merit
7 in Fig. 5; they are indicated by lines. These are calculated
8 assuming SiC resonators with a fixed thickness of 250 nm.
9 In the upper right is the thermoelastic limit for devices
10 (with intrinsic stress 1.5 GPa) of lengths ranging from 200
11 µm (left end) to 1000 µm (right end). Note that this
12 confirms that the resonators reported in [6] are operating
13 close to their material limit. Note also that the extensive
14 presence of crystalline defects needs to be factored in for
15 such hetero-epitaxial SiC films. The remaining lines
16 correspond to calculations incorporating clamping losses
17 according to [98] for four combinations of resonator width
18 and substrate thickness. These indicate that the beam
19 should be thin and the substrate thick to maximise $Q \times R$
20 and $Q \times f_1$. Damping mechanisms are discussed further in
21 Section 6.
22 The dynamic detection mode of nanoresonators has to
23 date made possible the detection of a single cell [99],
24 single virus [100], single DNA molecule [101], single
25 protein [73], and masses down to small zeptograms [81, 90,
26 102]. The following subsection includes transduction
27 techniques used for the dynamic actuation and sensing of
28 microbeam devices.
29
30
31 **4.2.2 Transduction techniques** A dynamic reso-
32 nant sensor further includes components such as an excita-
33 tion unit, a detection unit, and feedback circuitry. The
34 feedback circuitry is added to the system to ensure the res-
35 onator operates at the desired resonant frequency. For this,
36 the system requires an excitation unit to bring the resonator
37 to vibration and a detection unit to measure and detect the
38 resonant frequency and its motion [14].
39 The actuation/read-out mechanism selection is based
40 on the resonator type, geometry, material, and the expected
41 response magnitude. The frequency shift measurements of
42 microbeams are obtained through different forms of actua-
43 tion and detection schemes such as: electrostatic excitation
44 and capacitive detection [103, 104], magnetic excitation
45 and inductive detection [105], piezoelectric excitation and
46 detection [106, 107], electrothermal excitation and piezore-
47 sistive detection [108-111], hard contact/tunnelling detec-
48 tion [11, 69], and optical detection [101, 112].
49
50 **Electrostatic actuation and capacitive detec-
51 tion** Electrostatic excitation is performed by applying a
52 combination of both alternating and direct voltage on two
53 contacts/electrodes. This creates a periodic electrostatic
54 force within the resonator. This method is favourable for
55 integrated MEMS/NEMS devices because it is fast, simple,
56 easy to control, and requires low-power consumption [2].
57 This technique is typically combined with capacitive [113]
58 or tunnelling detection [114] mechanisms [32].
59
60
61
62
63
64
65

Capacitive detection is mainly used for non-liquid mass detection, where the resonator is placed close to a parallel electrode that is fixed to a substrate. The motion of the resonator will modulate the structure's capacitance, which can be measured electrically [2].

Magnetic actuation and detection This method is favourable for NEMS due to its easy fabrication and integration steps; a static magnetic field is applied perpendicular to the resonator through which an alternating current is running, resulting in the generation of a Lorentz force in the out-of-plane direction. This further results in the excitation of the resonator [77]. Longitudinal vibration cannot be excited with this mechanism since the Lorentz force only results in the perpendicular movement of the resonator [3]. Magnetic or inductive sensing can be combined with this actuation technique. The drawback of this sensing is that the resonator requires the supply of a magnetic field, which limits its on-chip applications [2].

Piezoelectric actuation and detection Piezoelectric materials can be used for both device actuation and readout purposes. Suitable piezoelectric elements include PZT (lead zirconate titanate), ZnO (zinc oxide), and AlN; AlN is also cleanroom compatible [32]. The beam resonator is mounted on an external piezoelectric element and is vibrated at a given frequency [32]. Alternatively, the piezoelectric material may be deposited directly onto the resonator, although this further complicates the fabrication [2]. Piezoelectric read-out is scalable with low power consumption, but it requires large thicknesses of piezoelectric element to obtain a large output signal [69].

Electrothermal actuation and piezoresistive detection In this case, the MEMS/NEMS resonator is excited as the result of the stress produced from the electrical heating. The mechanical strain is formed as the result of the thermal expansion coefficient differences between the electrode and the resonator, from a temperature gradient within the resonator's thickness, or a combination of both mechanisms.

The applied stress further changes the bulk resistivity. The resistance change is measured by placing the resonator in a Wheatstone bridge configuration. When voltage is applied to the bridge, the resistance variation can be measured. This mechanism can be performed in both gas and liquid media.

The piezoresistive mechanism is simple but requires extra electrical circuitry. Additional heat dissipation can also occur as the result of the current flow within the resonator [69]. This technique can be applied for epitaxial SiC resonators as 3C-SiC is a piezoresistive material [42].

Tunnelling/ hard contact detection If the resonator is placed very close to a counter electrode and a bias voltage is applied between them there will be a current

Copyright line will be provided by the publisher

flow which depends sensitively on the gap, and thus the motion of the resonator. The drawback of this technique is its fabrication difficulty. In the case of the hard contact detection, the resonator can touch the electrode [32].

Optical detection Optical detection is the most commonly used NEMS/MEMS detection mechanism due to its absence of electrical connections, sub-nanometre resolution, and reliability. The two most common methods are the 'optical lever' and optical interferometry [2, 69].

In an 'optical lever' light is reflected from the resonator onto a position-sensitive photodiode. Laser diodes or LEDs are mainly used to generate the beam light. Resonator motion shifts the reflected light's position on the photodiode and thus the collected energy, which can be measured. Interferometric detection is based on the interferences that happen when a beam of light reflects from two surfaces [52]. Optical interferometry has higher bandwidths and thus higher resolution than the optical lever method [2, 69].

Optical methods are not suited for liquid environments and can have complex design systems. Also, the detection of cantilevers with intrinsic bending is difficult because it complicates the optical alignment [32].

In both methods, piezoelectric materials can be used to excite the oscillator. We have used PZT element and Mach-Zehnder optical interferometry to measure the mechanical performance (*f* and *Q*) of our SiC resonators, as reported in [6, 115].

5 Dynamic sensing parameters

The following subsections explain the fundamentals of the dynamic sensing namely, frequency and quality factor.

5.1 Frequency

The out-of-plane flexural resonant frequencies of a rectangular microbeam consisting of a uniform material are described by Euler Bernoulli beam theory [76, 105]:

$$f_n = \frac{\kappa_n^2}{2\pi}\sqrt{\frac{k}{m}} = \frac{\kappa_n^2}{2\pi L^2}\sqrt{\frac{EI}{\rho A}} = \frac{\kappa_n^2 t}{4\pi\sqrt{3}L^2}\sqrt{\frac{E}{\rho}}, \quad (7)$$

where m and k are the beam's mass and spring constant, $\kappa_n^2/4\pi\sqrt{3}$ is the clamping coefficient, and κ_n is the eigenvalue; $\kappa_n = (n+1/2)\pi$ for bridges and $\kappa_n = (n-1/2)\pi$ for cantilever resonators. Thus, the clamping coefficient of the fundamental mode is 1.03 for the bridge and 0.162 for the cantilever. As mentioned earlier, it is necessary to replace E with $E(1-v^2)^{-1}$ when $w \geq 5t$. The in-plane flexural frequency equation differs from the out-of-plane in the I/A ratio, where for the out-of-plane movements: $I/A = t^2/12$ and for the in-plane movements $I/A = w^2/12$ [88]. Therefore, the mechanical frequency of a flexural beam is influenced by the geometry, mode number, and material properties.

For a beam with two layers of different materials, the resonant equation is modified to

$$f_n = \frac{\eta}{L^2}\left(\frac{E_1 I_1 + E_2 I_2}{\rho_1 A_1 + \rho_2 A_2}\right), \quad (8)$$

where η is a constant depending on the resonator mode number and boundary conditions; η = 3.57 for the fundamental mode of a double-clamped beam. This model is generally applied when a metal layer is deposited on the resonator surface. The model can be further extended to higher number of layers by adding the respective material $EI/\rho A$ term [3, 105].

A strain-dependent correction of the Euler Bernoulli theory becomes important in the presence of residual mean (tensile) stress within the resonator material; for out-of-plane double-clamped microresonators Eq. (7) is modified to Eq. (9) [3, 43, 116],

$$f_n = \frac{\kappa_n^2 t}{4\pi\sqrt{3}L^2}\sqrt{\frac{E}{\rho}}\sqrt{1+\gamma_n\frac{\sigma L^2}{Et^2}}, \quad (9)$$

where γ_n is a mode-dependent coefficient ($\gamma_n = 12(\kappa_n - 2)/\kappa_n^3$) and σ is the film tensile mean stress. It can be seen from Eq. (7) that higher frequencies can be achieved when having higher Young modulus to density ratio, thickness, and smaller length ($f \propto (t/L^2 \cdot \sqrt{E/\rho})$). This is always true for bulk or homoepitaxial microresonators. Conversely, for heteroepitaxial thin films such as 3C-SiC with $\gamma_n \sigma L^2/Et^2 >> 1$, the frequency is mainly a function of tensile stress and length ($f \propto \sqrt{\sigma}/(\sqrt{\rho} \cdot L)$). The frequency is not a function of thickness anymore and so thinner and lighter resonators may be fabricated.

The change in the frequency ($f^{+\Delta m}$) as the result of an added mass for the flexural beams can be obtained from [52]:

$$f_n^{+\Delta m} = \frac{\kappa_n^2}{4\pi\sqrt{3}}\sqrt{\frac{k}{m+\Delta m}}. \quad (10)$$

The torsional frequencies of a beam resonator is obtained from Eq. (11), where $G = E/(2(1+v))$, and $I = (tw^3 + wt^3)/12$ [88]. Similarly, the longitudinal frequencies of a resonator can be obtained from Eq. (12) [3]. The longitudinal modes have much higher resonant frequencies than the flexural modes as can be seen from the comparison between the respective equations.

$$\xi = \frac{t^4}{3}\left(\frac{w}{t} - \frac{192}{\pi^5}\sum_{n=1}^{\infty}\frac{1}{n^5}\tanh\frac{n\pi w}{2t}\right),$$

Copyright line will be provided by the publisher

1
2
3
4
5
6
7
8
9
10
11
12
13
14
15
16
17
18
19
20
21
22
23
24
25
26
27
28
29
30
31
32
33
34
35
36
37
38
39
40
41
42
43
44
45
46
47
48
49
50
51
52
53
54
55
56
57
58
59
60
61
62
63
64
65

$$f_n = \frac{2n-1}{4L}\sqrt{\frac{G\xi}{\rho I}} \tag{11}$$

$$f_n = \frac{n}{2L}\sqrt{\frac{E}{\rho}} \tag{12}$$

Finite element modelling (FEM) and simulation can be used to accurately predict the resonant frequencies based on the material properties, geometry, and clamping condition of the resonator prior to fabrication. The gradient stress within the epitaxial double-clamped SiC beam resonator can be modelled by subdividing the resonator film into multiple layers with particular thicknesses and assigning the specific measured mean stress to each layer [38, 117].

5.2 Quality factor Q is defined as the stored vibrational energy over the energy loss per cycle of vibration and is measured using techniques such as harmonic excitation, thermomechanical noise, wave propagation, and free decay. In the harmonic excitation method, Q is obtained from Eq. (13), where Δf_{-3dB} is the -3dB-power bandwidth of the resonance peak. In this case, Q indicates the narrowness of a resonance peak [12, 118]:

$$Q = \frac{f}{\Delta f_{-3dB}}. \tag{13}$$

Alternatively, Q can be obtained by fitting the resonance peak in the thermoelastic noise spectrum or from the attenuation of an elastic wave's amplitudes with a wavelength [119]. In the free decay method, Q is quantified from the time constant (τ_d) of the resonator's exponentially decaying amplitude during a ring-down process [69, 120]:

$$Q = \pi\tau_d f. \tag{14}$$

It is desirable for a resonator to have a high quality factor. This reduces the mechanical coupling to the surrounding environment, which further results in high accuracy, high resolution and spectral purity, and long-term stability [92, 121]. Also, lower energy is required to maintain the vibration in high Q [122, 123]. Q-factor is inversely proportional to damping parameters. The following section describes the influence of the damping parameters on the microbeam resonators' frequency, quality factor, and sensitivity. It also includes an overview of the methods that can be used to improve the sensitivity parameter ($Q \times f$) of epitaxial SiC microbeam resonators.

6 Damping Damping refers to the energy dissipation in the resonator and its impact on the mechanical performance of the resonator. Its influence on the mechanical frequency and Q-factor of microbeams are shown below. It should be noted that all the models shown in this section are for the flexural out-of-plane movements unless specified otherwise.

6.1 Damping on frequency For a resonator operating in a fluid other than air, its effective inertia increases as the result of the surrounding fluid. This results in a reduction in the fluid frequencies (f_F) as compared with the respective vacuum frequencies (f) as shown in Eq. (15), where ρ_F and μ_F are the fluid density and viscosity, and K is a free fitting parameter [52]:

$$\frac{f_F}{f} = \left(1 + \frac{\pi\rho_F w}{12K^3\rho t} + \frac{3\sqrt{\pi\mu_F\rho_F}}{4K^2\rho t\sqrt{f_F}}\right)^{-1/2}. \tag{15}$$

6.2 Damping and quality factor The magnitude of damping is influenced by many parameters including the resonator type, geometry, clamping, mode of vibration, and material (chemistry, defects, residual stress, crystallinity, surface, and interface). The damping of a resonator could also be influenced by temperature, pressure, processing steps, and transduction technique [12]. In general, damping is classified into medium damping (Q^{-1}_{Medium}), which is related to the environment of the resonator structure; clamping loss (Q^{-1}_{Clamp}), which is related to the energy dissipation through the resonator's anchors; material damping (Q^{-1}_{Mat}), which is related to the resonator material; and other losses [3, 14]:

$$\frac{1}{Q} = \sum\frac{1}{Q_{Medium}} + \sum\frac{1}{Q_{Clamp}} + \sum\frac{1}{Q_{Mat}} + \sum\frac{1}{Q_{Other}}, \tag{16}$$

where the major losses control the overall Q. Material losses including friction, and fundamental losses (including thermoelastic loss) [124-127] are rather low in MEMS, and their contribution to the total damping is negligible compared to the extrinsic losses. Material damping becomes important only after eliminating or minimizing the extrinsic losses [3]. Other losses include electrical charge damping as the result of trapped charges on the resonator, magnetomotive damping as the result of eddy current induced by external magnetic field in resistive elements, packaging and full scale device preparation losses [12, 94, 128].

6.2.1 Medium damping Most resonators are designed to operate in vacuum conditions. Nevertheless, it is important to understand how the Q-factor varies with fluid damping because medium damping is the most significant source of energy loss in MEMS [122, 129, 130].

The medium could be a viscous liquid in which the resonator is immersed, a viscous fluidic that flows within the resonator (microchannel), or a gas. Viscous damping is theoretically and experimentally understood and typically

Copyright line will be provided by the publisher

yields a very low Q. The Q is of the order of unity for the fundamental mode and increases with mode number [131, 132]. In addition to low Q, resonators immersed in liquids entrain fluid, effectively adding additional mass which reduces the mass sensitivity [133]. Low sensitivity limits the application of microresonators in liquid solutions. To overcome this problem, the microresonator can be used as a part of a self-oscillating system with a positive feedback. This way, the output can be amplified and fed back to the system. The apparent Q-factors obtained from this scheme are two to three orders of magnitude above the intrinsic Qs [69, 134].

In addition, resonators can be used as microchannels operating in vacuum, where a liquid can flow inside the resonator and thus Q can be enhanced. This configuration has been used for applications such as density and viscosity measurements [135, 136]. Viscous fluidic damping is also theoretically obtained [137].

Gas damping is another form of medium damping. Newell was the first to analyse the effect of air damping on the Q [10]. He divided the pressure range from ambient pressure to vacuum into three regions, namely, viscous, molecular (fine vacuum), and intrinsic (high vacuum).

The intrinsic region is where the pressure is very low so that air damping is negligible and thus Q is independent of the pressure. This region's upper boundary (critical pressure: P_c) varies depending on the microresonator material, dimension, shape, and mode of vibration [12, 83, 138], To find the upper boundary of the intrinsic region experimentally, the resonator needs to be operated at different pressures. The function $Q = 1/((1/Q_0) + \alpha P)$ can then be used for analysis; Q_0 is the intrinsic Q-factor and α is a fitting factor. The device is operating in the intrinsic region when the αP factor is smaller than Q_0 [115].

At higher pressure the air molecules are still too far apart to interact but they do significantly damp the oscillator by colliding with it. In this molecular case it is predicted that $Q \propto 1/P$ [52, 130, 138].

Last, in the viscous region, the air molecules can interact with each other [122, 130]. The transition between viscous and molecular regions is determined by the Knudsen number (K_n), which is the ratio of the gas mean free path (λ_f) to the length scale of the resonator (L_r). K_n>1 indicates that the resonator is in the molecular region and K_n<1 shows that the resonator is in the viscous regime. The mean free path is obtained from

$$\lambda_f = k_B T \Big/ \sqrt{2}\pi P d_{gas}^2 , \tag{17}$$

where k_B is the Boltzmann constant and d_{gas} is the gas molecule diameter [139].

6.2.2 Clamping loss When operating in a high vacuum, the viscous damping from the environment can be eliminated [129, 140]. This makes the clamping loss (Q_{Clamp}^{-1}), which is the result of energy propagation from the beam resonator anchors to the substrate [141], one of the dominant dissipation factors. It is important for a beam resonator to have perfect-clamped anchors and thus a fixed center of gravity, because an unbalanced resonator would have energy losses at its anchors due to the coupling between the resonator and the surrounding material [14, 142].

The clamping loss is strongly geometry dependent. There are few known theoretical models to calculate the clamping loss of a beam resonator, which could greatly assist in design of the resonator with minimized clamping loss even though these theoretical models differ slightly with the real applications [98]. Cantilever clamping loss model was first reported by Jimbo and Itao in 1968: $Q_{Clamp}^{-1} \propto (t/L)^3$ [143]. Later in 2001, Cross and Lifshitz [144] modelled the Q_{Clamp}^{-1}, assuming that the beam is two-dimensional as shown in Eq. (18). They also modelled the in-plane movements as shown in Eq. (19).

$$\text{Out-of-plane: } Q_{Clamp}^{-1} \propto t/L \tag{18}$$

$$\text{In-plane: } Q_{Clamp}^{-1} \propto (w/L)^3 \tag{19}$$

The three-dimensional models for the beam were later introduced by Photiadis and Judge, where support thickness is also considered [145]: Their equation is approximated to Eq. (18) for the perfect-clamped beams.

Q_{Clamp}^{-1} can be reduced through the minimization of chip (piezoelectric actuator) and substrate contact, vibration isolators [146], and acoustic reflectors [147]; alternatively more complicated structures such as free-free beams (where anchors are connected to the beam nodal points) [148] or phononic bandgap resonators [149, 150] can assist in reducing Q_{Clamp}^{-1}.

6.2.3 Material damping Material damping refers to all the losses related to the resonators' volume, surface, and any internal interfaces (layer, grain, or phase boundaries). Material loss is further divided to two forms of friction losses (surface loss (Q_{Surf}^{-1}) and internal friction loss (Q_{IF}^{-1})) and fundamental losses (such as thermoelastic loss: Q_{TED}^{-1}). Friction losses arise from material imperfections while fundamental losses are the result of the interaction between the resonator's strain field, photons, and electrons during its vibration. Q_{TED}^{-1} sets the ultimate lower limit on damping for MEMS resonators [12, 98].

Surface loss arises when surface atoms are different than those of the bulk or as the result of surface roughness [120, 151]. Possible sources of surface dissipation are adsorbents on the surface or surface defects during fabrica-

Copyright line will be provided by the publisher

tion. Surface loss can be minimized or eliminated through surface treatment techniques. In the case of surface loss being the dominant loss factor, Q is obtained from [98, 120, 152]:

$$Q_{Surf} = \beta t, \quad (20)$$

where $\beta = E/(6t_{ls}E''_{ls})$ for $w >> t$, with t_{ls} and E''_{ls} being the thickness and the Young modulus of the surface layer. Villanueva and Schmid calculated β = 6×10^10 ± 4×10^10 for αSiN membranes [151]. On the contrary, the internal friction loss is caused by the motion of the crystallographic defects and thus its magnitude is dependent on the type, density, distribution, mobility and the interactions of the defects [12]. This damping could be reduced by using high quality single-crystal materials, improving the fabrication processing steps, and by reducing the operation temperature [153, 154]. In the case of epitaxial monocrystalline SiC resonators, SiC backside etching and removal of its defective portion can help to improve the crystal quality and thus reducing the internal friction loss greatly.

The internal friction loss is less in ceramic materials, and in alloys as compared to pure metals due to their lower defects mobility [155]. The friction loss is obtained from:

$$Q_{IF}^{-1} = Tan\delta(\omega) = \frac{\Delta E(\omega\sqrt{\tau_\sigma + \tau_\varepsilon})}{\sqrt{E_r E_u}\,(1+\omega^2(\sqrt{\tau_\sigma + \tau_\varepsilon})^2)}, \quad (21)$$

where δ is the phase lag between the strain and the stress within the resonator's material and *tan* δ is the loss tangent; ω is the circular (angular) natural frequency; E_r and E_u are the relaxed and unrelaxed Young modulus and $\Delta E = E_u - E_r$; and τ_σ and τ_ε are the relaxation times at constant stress and strain, respectively. The internal friction has its minimum at $\omega\sqrt{\tau_\sigma + \tau_\varepsilon} = 1$, which is the maximum point of the Q_{IF} peak (Debye peak): $Q_{IF,\max} = \Delta E/(2\sqrt{E_r E_u})$. Debye dissipation peaks occurs for many other relaxation mechanisms such as thermoelastic relaxation as well [98, 156].

Finally, thermoelastic dissipation (TED) is the result of coupling between the resonator's strain field and the local temperature[124, 157]. As the resonator vibrates regions under compression will become warm whilst regions under expansion will be cool. The resulting temperature gradient causes energy flow from the warmer region to the cooler region, resulting in an irreversible energy loss [91, 120].

Q_{TED}^{-1} reduces with thickness. The rate of energy loss depends on the material properties following Liftshitz and Roukes' work [124]:

$$\xi = t\sqrt{\frac{2\pi f_n c_v}{2\kappa}},$$

$$Q_{TED} = \frac{c_v}{ET\alpha^2}\left(\frac{6}{\xi^2} - \frac{6}{\xi^3}\frac{\sinh\xi + \sin\xi}{\cosh\xi + \cos\xi}\right)^{-1} \quad (22)$$

where T is the temperature (300 K). This theoretical expression makes it possible to determine how closely a given string is operating to the thermoelastic limit. The literature reported values of these properties for most of the semiconductor materials used in MEMS including epitaxial SiC films are shown in Table 1.

A resonator operating in high vacuum can approach the ultimate theoretical limit when the dissipation sources such as viscous, clamping, surface, and internal friction are reduced or eliminated. However, as mentioned earlier, the resonator Q is also affected by inevitable further factors such as functionalization, metallization, and packaging processes to build a full scale device [12].

A metallization process is required for electrical actuation and readout purposes of MEMS resonators. However, the addition of even a thin metal layer severely degrades the Q due to the large friction losses it induces [158, 159]. This damping can be reduced by an annealing process to improve the crystal quality [153], by reducing the metal film thickness [127], and by alloying the metal [155]. Likewise, the damping can be mitigated by removing the metal from the resonator's clamping regions and regions with high strain, but with the cost of adding difficulty to the fabrication and integration steps [160, 161]. Another method is to replace the conventional metallic overlayer with graphene; graphene is the lightest material ever made, and boasts extremely high electrical and thermal conductivity. It is reported that the Q degradation is much less for a graphene overlayer than a conventional metal [162]. In the case of epitaxial SiC, graphene can be grown on the surface of the SiC film directly and transfer-free due to the presence of the carbon atoms [163-165].

6.2.4 Damping dilution in string resonators To further improve the Q, it is important to select the appropriate beam resonator type. Compared to bridge resonators, cantilevers have higher Q-factors in general due to their reduced clamping points [102, 141]. However, the bridge resonators achieve much higher Q when there is residual (tensile) mean stress within the resonator's material. The tensile stress can be generated within the material as the result of the epitaxial growth [6, 83, 97, 166], bending of the substrate chip [95, 167], electrostatic forces, and stiction [168]. Verbridge *et al.* were the first to discover the impact of tensile stress on the mechanical Q of d-c string resonators [92]. The influence of tensile stress on Q is also confirmed by other works using αSiN [93], GaAs [97], and Al [95],and our recent report on SiC [6]. A summary is shown in Table 2.

This increase in Q is related to the increased stored elastic energy as the resonator requires more energy to

Copyright line will be provided by the publisher

work against the tensile stress during the vibration ($W_{tensile}$) [169]. Thus [93]:

$$Q = 2\pi \frac{W_{tensile} + W_{elongation} + W_{bending}}{\Delta W_{elongation} + \Delta W_{bending}}, \quad (23)$$

where $W_{elongation}$, $\Delta W_{elongation}$, $W_{bending}$, and $\Delta W_{bending}$ are the stored and lost energy due to elongation and bending, respectively. Consequently, for resonators in their intrinsic loss limit Q can be described by [98, 151]:

$$Q = \alpha_{dd} \cdot Q_{Mat}, \quad (24)$$

where α_{dd} is the damping dilution factor, which has a value larger than unity because $W_{tensile}$ is typically much larger than the other stored energies. For long ($L >> t$) resonators operating in their fundamental flexural mode, α_{dd} can be simplified to [98, 151]

$$\alpha_{dd} = \frac{L}{t}\left(\frac{3\sigma}{E}\right)^{1/2}. \quad (25)$$

6.3 Temperature effect Material properties and resonator geometry can vary as the result of temperature variation. For instance, the Young modulus is temperature dependent, and thermal expansion generally forces the resonator geometry to change with temperature variations [52]. As the result, it is important for the resonator to operate at a fixed temperature and for MEMS to have a low temperature sensitivity to ensure accurate measurements and sensing. It should be noted that different resonator modes respond to temperature changes differently. The overall effect of temperature variations is often dependent on the details of excitation and detection techniques used [14].

7 Mean stress influence on mass sensitivity of SiC flexural microbridge resonators As mentioned earlier, tensile stress enhances the mass sensitivity of double-clamped resonators; the mean stress is released because of the free end in the case of single-clamped resonators. In the case of out-of-plane flexural string resonators (in their intrinsic limit) the mass sensitivity is analysed through the $f_n \times Q$ figure of merit, where $f_n \propto \left(\sqrt{\sigma}/L\right)$ and $Q = \sqrt{3\sigma}L/(t\sqrt{E}) \cdot Q_{Mat}$ following Eq. (9) and Eq. (24). It should be noted that E can be affected by the defect density and its value decreases as thickness reduces for epitaxial films [170-172]. Therefore, it is true to say that tensile stress is the main parameter that can be used to increase both f_n and Q parameters and thus the $f_n \times Q$ product. From Table 2, we can observe that tensile stress values as high as 1500 MPa can be achieved for epitaxial SiC strings and for the <111> orientation, with $Q \times f_1$ product exceeding state-of-the-art αSiN microstrings.

Our analysis on the SiC(100) and SiC(111) string resonators of similar geometries showed that Q is similar for both orientations even though SiC(111) has higher tensile stress value. We related this to the fact that the SiC(100) film has a much better crystal quality and thus lower friction losses as compared to the SiC(111) film. However, SiC(111) string resonators still have higher $f_n \times Q$ products due to their higher resonant frequencies [115].

8 Gradient stress impact on SiC cantilever static behavior Gradient stress influences the static performance of cantilever resonators. This further limits the cantilever resonators' application range. Therefore, it is important to understand and be able to engineer the bending according to the specific application.

Gradient stress can be tensile (+) or compressive (-). In the case of positive gradient, the film will have a concave appearance due to its inclination to contract. Whereas, for compressive gradient stress, the film will try to expand, causing the substrate to bow in a convex manner [2]. The deformation can be observed through the intrinsic bending of the released cantilever resonators [25, 28, 57, 173]. Three possible forms of cantilever intrinsic bending as the result of stress distribution and gradients are shown in Fig. 6, where the dashed line is located at the centre of the beams.

The cantilever intrinsic bending is beneficial for many MEMS applications such as micro-tweezers [174, 175],

Table 2 Literature study on the mechanical behaviour of the MEMS bridges in vacuum.

Ref.	Material	L (µm)	w (µm)	t (nm)	σ (MPa)	P (mbar)	f_1 (kHz)	Q	$Q \times f_1$ (Hz)	$Q \times R$ (nm^{-1})
[6]	SiC(111)	1000	4	255	750	2×10^{-7}	220	8×10^{5}	1.8×10^{11}	6.7×10^{3}
[6]	SiC(111)	930	4	255	1500	10^{-6}	280.5	3×10^{6}	8.4×10^{11}	2.5×10^{4}
[93]	αSiN	1553	4	177	190	10^{-5}	78.7	2×10^{6}	1.6×10^{11}	2.4×10^{4}
[93]	αSiN	1553	4	157	890	10^{-5}	176	3×10^{6}	5.3×10^{11}	4.0×10^{4}
[97]	GaAs	37	10	200	0	-	1230	1800	2.2×10^{9}	18.4
[97]	GaAs	53	10	200	**	-	2900	2×10^{3}	5.5×10^{10}	20.4
[95]	Al	5	3	10	0	$<10^{-3}$	1320	720	9.5×10^{8}	144
[95]	Al	5	3	10	13.5	$<10^{-3}$	1370	1.4×10^{3}	1.9×10^{9}	281

**strained 0.35% along the beam

Copyright line will be provided by the publisher

1
2
3
4
5
6
7
8
9
10
11
12
13
14
15
16
17
18
19
20
21
22
23
24
25
26
27
28
29
30
31
32
33
34
35
36
37
38
39
40
41
42
43
44
45
46
47
48
49
50
51
52
53
54
55
56
57
58
59
60
61
62
63
64
65

micro-cages [176], micro-wrappers [177], and fibre optic switches [178, 179]. At the same time, flat cantilevers are required for most microsensors [32, 69]. Different methods are reported for tailoring the gradient stress within the epitaxial films and thus the cantilever intrinsic bending, such as variation in growth parameters [25, 180], metallization process [26, 27, 181], and application of multilayer structures [182].

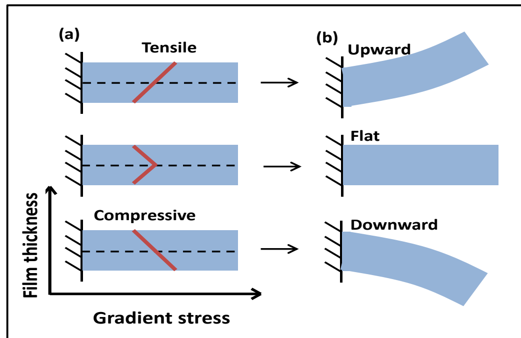

Figure 6 (a) Stress gradients within the epitaxial film (red line) and (b) intrinsic bending behaviours of released cantilevers as the result of gradient stresses. For simplicity a linear gradient is assumed.

We reported a simple method to control and tailor the intrinsic bending of epitaxial SiC cantilever by combining the knowledge of the film gradient stress (in nanometer resolution) [38] with finite element modelling and through the appropriate selection of geometry and film type. We observed through FEM modelling and experimentally (with very good agreement level) that we could achieve upward, almost zero, and downwards deflection with varying bending degree for our SiC(100) films with thicknesses of below 80 nm, ~80 nm, and above 80 nm, respectively. This is further related to the fact that, as shown in our nanometre-resolution stress model [38], the dominant gradient stress is tensile below 80 nm thickness and compressive above 80 nm thickness. The bending degree further increases as the result of the increase in the gradient stress and the cantilever length. As for the SiC(111) cantilever, the bending remains upward for any thickness up to the maximum investigated (250 nm) because the stress gradient remains tensile throughout [117]. Figure 7 show the deflection comparison between SiC(111) and SiC(100) cantilevers with 250 nm thickness.

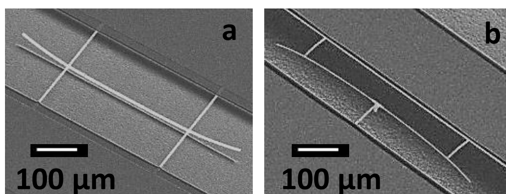

Figure 7 Intrinsic bending of (a) SiC(111) and (b) SiC(100) freefree beam resonators with 250 nm thickness.

9 Further applications Microbeam resonators are applied for the detection of volatile organics [183], glucose [184, 185], DNA hybridization [59], bacteria and viruses [99, 186, 187] with unparalleled sensitivities. On top of that, due to their low thermal mass, microbeams are used in explosives detection via local differential thermal analysis. Using this method, a thermal fingerprint can be achieved for each explosive material according to the material phase transition upon heating [188, 189]. Another application of microbeams is in material characterization and for the measurements of materials properties [190].

Epitaxial SiC sensors could be further applied in fields such as: power plants, combustion control, automotive and aerospace applications that require high temperature operation or operation in radiative and corrosive environments [2, 41, 191]; and food and medical sensors due to their biocompatibility and chemical inertness [5, 192, 193]. This, again, provided the SiC/silicon interface challenge is successfully addressed.

10 Conclusion Microbeam resonators applications are expanding and thus higher mass sensitivity is in demand. We reviewed the parameters influencing the mass sensitivity parameter and the approaches required to further optimize the sensitivity of epitaxial SiC beam resonators. This included an in-depth analysis on the frequency, damping parameters, and material properties. The epitaxial SiC microstrings' sensitivities can approach their thermoelastic theoretical limits by (1) high vacuum operation; (2) reduction of clamping loss through the application of perfect-clamped anchors, clean from any residues; (3) reduction of friction loss by improving the resonator's crystal and surface quality and by removing the defective layer from the backside of the epitaxial SiC film; and (4) using high tensile stress. We emphasized that epitaxial SiC microstrings outperform other wide bandgap materials in terms of resonant performance reported at this point. Besides that, epitaxial SiC has easy micromachining process and is biocompatible. In addition, we reviewed the methods used to tailor the intrinsic bending of cantilever resonators, including epitaxial SiC cantilevers, in order to increase their application range.

Acknowledgements The authors acknowledge the support from AFOSR through the AOARD 15IOA053 grant and the Australian Research Council through the Discovery Project No. DP140100734. Assoc. Prof. Francesca Iacopi and Assoc. Prof. Warwick P. Bowen are the recipients of Australian Research Council Future Fellowship (FT120100445 and FT140100650, respectively). We also acknowledge the use of ANFF infrastructure at the Queensland node.

References

[1] N. G. Wright and A. B. Horsfall, Material Matters **4**, 5 (2009).

Copyright line will be provided by the publisher

[2] V. Cimalla, J. Pezoldt, and O. Ambacher, J. Phys. D: Appl. Phys. **40**, 6386 (2007).
[3] K. Brueckner, F. Niebelschuetz, K. Tonisch, C. Foerster, V. Cimalla, R. Stephan, J. Pezoldt, T. Stauden, O. Ambacher, and M. A. Hein, Phys. Stat. Sol. (a) **208**, 357-376 (2011).
[4] C. A. Zorman and R. J. Parro, Phys. Stat. Sol. (b) **245**, 1404-1424 (2008).
[5] A. Oliveros, A. Guiseppi-Elie, and S. E. Saddow, Biomed. Microdevices, 1-16 (2013).
[6] A. R. Kermany, G. Brawley, N. Mishra, E. Sheridan, W. P. Bowen, and F. Iacopi, Appl. Phys. Lett. **104**, 081901 (2014).
[7] A. Severino, C. Locke, R. Anzalone, M. Camarda, N. Piluso, A. La Magna, S. Saddow, G. Abbondanza, G. D'Arrigo, and F. La Via, ECS Trans. **35**, 99-116 (2011).
[8] P. M. Sarro, Sens. Actuators A: Phys. **82**, 210-218 (2000).
[9] H. C. Nathanson, W. E. Newell, R. A. Wickstrom, and J. R. Davis Jr, IEEE Trans. Electron Devices **14**, 117-133 (1967).
[10] W. E. Newell, Science **161**, 1320-1326 (1968).
[11] G. Binnig, C. F. Quate, and C. Gerber, Phys. Rev. Lett. **56**, 930 (1986).
[12] S. Joshi, S. Hung, and S. Vengallatore, EPJ Tech. Instrum. **1**, 5 (2014).
[13] R. M. Langdon, J. Phys. E. **18**, 103 (1985).
[14] G. Stemme, J. Micromech. Microeng. **1**, 113 (1991).
[15] A. Ellison, J. Zhang, J. Peterson, A. Henry, Q. Wahab, J. P. Bergman, Y. N. Makarov, A. Vorob'ev, A. Vehanen, and E. Janzén, Mater. Sci. Eng., B **61**, 113-120 (1999).
[16] C. A. Zorman, A. J. Fleischman, A. S. Dewa, M. Mehregany, C. Jacob, S. Nishino, and P. Pirouz, J. Appl. Phys. **78**, 5136-5138 (1995).
[17] M. Syväjärvi, R. Yakimova, H. H. Radamson, N. T. Son, Q. Wahab, I. G. Ivanov, and E. Janzen, J. Cryst. Growth **197**, 147-154 (1999).
[18] J. Chen, A. J. Steckl, and M. J. Loboda, J. Vac. Sci. Technol., B **16**, 1305-1308 (1998).
[19] S. Nishino, J. A. Powell, and H. A. Will, Appl. Phys. Lett. **42**, 460-462 (1983).
[20] J. Eid and I. G. Galben, LMGP/INPG, (2008).
[21] L. Wang, S. Dimitrijev, J. Han, A. Iacopi, L. Hold, P. Tanner, and H. B. Harrison, Thin Solid Films **519**, 6443-6446 (2011).
[22] R. Anzalone, A. Severino, G. DArrigo, C. Bongiorno, G. Abbondanza, G. Foti, S. Saddow, and F. La Via, J. Appl. Phys. **105**, 084910-084910-084917 (2009).
[23] N. Mishra, L. Hold, A. Iacopi, B. Gupta, N. Motta, and F. Iacopi, J. Appl. Phys. **115**, 203501 (2014).
[24] F. Iacopi, G. Walker, L. Wang, L. Malesys, S. Ma, B. V. Cunning, and A. Iacopi, Appl. Phys. Lett. **102**, 011908 (2013).
[25] R. Anzalone, M. Camarda, C. Locke, D. Alquier, A. Severino, M. Italia, D. Rodilosso, C. Tringali, A. La Magna, and G. Foti, J. Electrochem. Soc. **157**, H438-H442 (2010).
[26] C. Zgheib, P. M. Masri, P. Weih, O. Ambacher, and J. Pezoldt, Mater. Sci. Forum **457-460**, 301-304 (2004).
[27] J. Pezoldt, R. Nader, F. Niebelschütz, V. Cimalla, T. Stauden, C. Zgheib, and P. Masri, Phys. Stat. Sol. (a) **205**, 867-871 (2008).
[28] R. Anzalone, G. D'arrigo, M. Camarda, C. Locke, S. E. Saddow, and F. La Via, J. Microelectromech. Syst. **20**, 745-752 (2011).
[29] M. Zielinski, J. F. Michaud, S. Jiao, T. Chassagne, A. E. Bazin, A. Michon, M. Portail, and D. Alquier, J. Appl. Phys. **111**, 053507 (2012).
[30] A. Pradeepkumar , Mishra, N., Kermany, A. R., Boeckl, J. J., Hellerstedt, J, Fuhrer, M. S., Iacopi, F. , Appl. Phys. Lett. **109**, 011604 (2016).
[31] S. Jiao, Y. Murakami, H. Nagasawa, H. Fukidome, I. Makabe, Y. Tateno, T. Nakabayashi, and M. Suemitsu, in: Mater. Sci. Forum, (Trans Tech Publ, 806, 2014), pp. 89-93.
[32] A. Boisen, S. Dohn, S. S. Keller, S. Schmid, and M. Tenje, Rep. Prog. Phys. **74**, 036101 (2011).
[33] B. El-Kareh, Fundamentals of semiconductor processing technology, (Springer Science & Business Media, 2012), p.
[34] K. E. Spear and J. P. Dismukes, Synthetic diamond: emerging CVD science and technology, (John Wiley & Sons, 25, 1994), p.
[35] P. A. Alekseev, M. S. Dunaevskii, A. V. Stovpyaga, M. Lepsa, and A. N. Titkov, Semiconductors **46**, 641-646 (2012).
[36] M. E. Levinshtein, S. L. Rumyantsev, and M. S. Shur, Properties of Advanced Semiconductor Materials: GaN, AIN, InN, BN, SiC, SiGe, (John Wiley & Sons, 2001), p.
[37] Y. U. Burenkov, Phys. Solid State **15**, 1175-1177 (1973).
[38] F. Iacopi, R. E. Brock, A. Iacopi, L. Hold, and R. H. Dauskardt, Acta Mater. **61**, 6533-6540 (2013).
[39] N. G. Wright, Kirk-Othmer; (John Wiley & Sons, Inc., New York, 2006), chap.
[40] L. Jiang and R. Cheung, Int. J. Comput. Mater. Sci. Surf. Eng. **2**, 227-242 (2009).
[41] N. G. Wright and A. B. Horsfall, J. Phys. D: Appl. Phys. **40**, 6345 (2007).
[42] H. P. Phan, D. V. Dao, K. Nakamura, S. Dimitrijev, and N. T. Nguyen, J. Microelectromech. Syst. **24**, 1663-1677 (2015).
[43] R. G. Azevedo, D. G. Jones, A. V. Jog, B. Jamshidi, D. R. Myers, L. Chen, X. A. Fu, M. Mehregany, M. B. J. Wijesundara, and A. P. Pisano, IEEE Sensors J. **7**, 568-576 (2007).
[44] M. Gad-el-Hak, MEMS: Design and fabrication, (CRC press, 2005), p. 2-17.
[45] J. M. Leger, J. Haines, and B. Blanzat, J. Mater. Sci. Lett. **13**, 1688-1690 (1994).
[46] R. D. Blevins and R. Plunkett, J. Appl. Mechanics **47**, 461 (1980).
[47] E. Carrera, G. Giunta, and M. Petrolo, Beam structures: classical and advanced theories, (John Wiley & Sons, 2011), p.
[48] S. P. Timoshenko, Philos. Mag. **43**, 125-131 (1922).
[49] J. C. Hsu, R. P. Chang, and W. J. Chang, Phys. Lett. A **372**, 2757-2759 (2008).
[50] S. P. Timoshenko, History of Strength of Materials, (Dover, New York, 1983), p.

Copyright line will be provided by the publisher

[51] S. Schmid, B. Malm, and A. Boisen, Micro Electro Mechanical Systems (MEMS), 2011 IEEE 24th International Conference on, 481-484 (2011).
[52] K. M. Goeders, J. S. Colton, and L. A. Bottomley, Chem. Rev. **108**, 522 (2008).
[53] P. A. Rasmussen, A. V. Grigorov, and A. Boisen, J. Micromech. Microeng. **15**, 1088 (2005).
[54] P. Lu, H. P. Lee, C. Lu, and S. J. O'shea, Phys. Rev. B: Condens. Matter **72**, 085405 (2005).
[55] D. Then, A. Vidic, and C. Ziegler, Sens. Actuators B: Chem. **117**, 1-9 (2006).
[56] R. Datar, S. Kim, S. Jeon, P. Hesketh, S. Manalis, A. Boisen, and T. Thundat, MRS Bull. **34**, 449-454 (2009).
[57] M. Bosi, B. E. Watts, G. Attolini, C. Ferrari, C. Frigeri, G. Salviati, A. Poggi, F. Mancarella, A. Roncaglia, and O. Martínez, Cryst. Growth Des. **9**, 4852-4859 (2009).
[58] M. Zielinski, A. Leycuras, S. Ndiaye, and T. Chassagne, Appl. Phys. Lett. **89**, 131906 (2006).
[59] J. Fritz, M. K. Baller, H. P. Lang, H. Rothuizen, P. Vettiger, E. Meyer, H. J. Güntherodt, C. Gerber, and J. K. Gimzewski, Science **288**, 316-318 (2000).
[60] R. McKendry, J. Zhang, Y. Arntz, T. Strunz, M. Hegner, H. P. Lang, M. K. Baller, U. Certa, E. Meyer, and H. J. Güntherodt, Proc. Natl. Acad. Sci. **99**, 9783-9788 (2002).
[61] M. Watari, J. Galbraith, H. P. Lang, M. Sousa, M. Hegner, C. Gerber, M. A. Horton, and R. A. McKendry, J. Am. Chem. Soc. **129**, 601-609 (2007).
[62] J. Mertens, C. Rogero, M. Calleja, D. Ramos, J. A. Martín-Gago, C. Briones, and J. Tamayo, Nat. Nanotech. **3**, 301-307 (2008).
[63] G. Wu, H. Ji, K. Hansen, T. Thundat, R. Datar, R. Cote, M. F. Hagan, A. K. Chakraborty, and A. Majumdar, Proc. Natl. Acad. Sci. **98**, 1560-1564 (2001).
[64] M. L. Sushko, J. H. Harding, A. L. Shluger, R. A. McKendry, and M. Watari, Adv. Mater. **20**, 3848-3853 (2008).
[65] F. Liu, Y. Zhang, and Z. Ou-Yang, Biosens. Bioelectron. **18**, 655-660 (2003).
[66] M. R. Begley, M. Utz, and U. Komaragiri, J. Mech. Phys. Solids **53**, 2119-2140 (2005).
[67] S. Singamaneni, M. C. LeMieux, H. P. Lang, C. Gerber, Y. Lam, S. Zauscher, P. G. Datskos, N. V. Lavrik, H. Jiang, and R. R. Naik, Adv. Mater. **20**, 653-680 (2008).
[68] J. H. He, S. Singamaneni, C. H. Ho, Y. H. Lin, M. E. McConney, and V. V. Tsukruk, Nanotech. **20**, 065502 (2009).
[69] N. V. Lavrik, M. J. Sepaniak, and P. G. Datskos, Rev. Sci. Instrum. **75**, 2229-2253 (2004).
[70] Z. Hu, T. Thundat, and R. J. Warmack, J. Appl. Phys. **90**, 427-431 (2001).
[71] H. P. Lang, M. Hegner, and C. Gerber, CHIMIA **56**, 515-519 (2002).
[72] D. Ramos, J. Tamayo, J. Mertens, M. Calleja, and A. Zaballos, J. Appl. Phys. **100**, 106105 (2006).
[73] A. K. Naik, M. S. Hanay, W. K. Hiebert, X. L. Feng, and M. L. Roukes, Nat. Nanotech. **4**, 445-450 (2009).
[74] E. Buks and B. Yurke, Phys. Rev. E: Stat. Phys., Plasmas, Fluids, **74**, 046619 (2006).
[75] M. H. Kim, D. Kim, J. B. Choi, and M. K. Kim, Phys. Chem. Chem. Phys. **16**, 15263-15271 (2014).
[76] J. S. Bunch, A. M. Van Der Zande, S. S. Verbridge, I. W. Frank, D. M. Tanenbaum, J. M. Parpia, H. G. Craighead, and P. L. McEuen, Science **315**, 490-493 (2007).
[77] K. L. Ekinci and M. L. Roukes, Rev. Sci. Instrum. **76**, 061101 (2005).
[78] R. T. Howe and R. S. Muller, IEEE Trans. Electron Devices **33**, 499-506 (1986).
[79] P. S. Waggoner and H. G. Craighead, Lab Chip **7**, 1238-1255 (2007).
[80] M. A. Taylor, A. Szorkovszky, J. Knittel, K. H. Lee, T. G. McRae, and W. P. Bowen, Opt. Express **20**, 12742-12751 (2012).
[81] K. L. Ekinci, Y. T. Yang, and M. L. Roukes, J. Appl. Phys. **95**, 2682-2689 (2004).
[82] C. M. Lin, Y. Y. Chen, V. V. Felmetsger, D. G. Senesky, and A. P. Pisano, Adv. Mater. **24**, 2722-2727 (2012).
[83] S. S. Verbridge, H. G. Craighead, and J. M. Parpia, Appl. Phys. Lett. **92**, 013112-013112-013113 (2008).
[84] X. M. H. Huang, X. L. Feng, C. A. Zorman, M. Mehregany, and M. L. Roukes, Nes J. Phys. **7**, 247 (2005).
[85] J. H. Ko, J. Jeong, J. Choi, and M. Cho, Appl. Phys. Lett. **98**, 171909 (2011).
[86] X. Liu, J. F. Vignola, H. J. Simpson, B. R. Lemon, B. H. Houston, and D. M. Photiadis, J. Appl. Phys. **97**, 023524 (2005).
[87] I. Bargatin, E. B. Myers, J. S. Aldridge, C. Marcoux, P. Brianceau, L. Duraffourg, E. Colinet, S. Hentz, P. Andreucci, and M. L. Roukes, Nano Lett. **12**, 1269-1274 (2012).
[88] A. W. McFarland, M. A. Poggi, L. A. Bottomley, and J. S. Colton, J. Micromech. Microeng. **15**, 785 (2005).
[89] K. Ekinci, X. Huang, and M. Roukes, Appl. Phys. Lett. **84**, 4469-4471 (2004).
[90] Y. T. Yang, C. Callegari, X. L. Feng, K. L. Ekinci, and M. L. Roukes, Nano Lett. **6**, 583-586 (2006).
[91] X. L. Feng, C. A. Zorman, M. Mehregany, and M. L. Roukes, Solid-State Sensor, Actuator and Microsystems Workshop, 86–89 (2006).
[92] S. S. Verbridge, J. M. Parpia, R. B. Reichenbach, L. M. Bellan, and H. G. Craighead, J. Appl. Phys. **99**, 124304 (2006).
[93] S. Schmid, K. D. Jensen, K. H. Nielsen, and A. Boisen, Phys. Rev. B: Condens. Matter **84**, 165307 (2011).
[94] A. Cleland and M. Roukes, Sens. Actuators A: Phys. **72**, 256-261 (1999).
[95] Y. J. Yi, Y. D. Kim, J. H. Bak, S. R. Lee, K. Heo, S. Hong, K. Char, and Y. D. Park, Curr. Appl. Phys. **11**, 746-749 (2011).
[96] A. Cleland, M. Pophristic, and I. Ferguson, Appl. Phys. Lett. **79**, 2070-2072 (2001).
[97] H. Yamaguchi, K. Kato, Y. Nakai, K. Onomitsu, S. Warisawa, and S. Ishihara, Appl. Phys. Lett. **92**, 251913 (2008).
[98] S. Schmid, Villanueva, L. G., and Roukes, M. L., in Fundamentals of Nanomechanical Resonators; Vol., ed., edited by (Springer International Publishing, 2016), p. 56-87.

Copyright line will be provided by the publisher

[99] B. Ilic, D. Czaplewski, M. Zalalutdinov, H. G. Craighead, P. Neuzil, C. Campagnolo, and C. Batt, J. Vac. Sci. Technol., B **19**, 2825-2828 (2001).
[100]A. Gupta, D. Akin, and R. Bashir, Appl. Phys. Lett. **84**, 1976-1978 (2004).
[101]B. Ilic, Y. Yang, K. Aubin, R. Reichenbach, S. Krylov, and H. G. Craighead, Nano Lett. **5**, 925-929 (2005).
[102]K. Jensen, K. Kim, and A. Zettl, Nat. Nanotech. **3**, 533-537 (2008).
[103]L. Sekaric, J. M. Parpia, H. G. Craighead, T. Feygelson, B. H. Houston, and J. E. Butler, Appl. Phys. Lett. **81**, 4455-4457 (2002).
[104]C. L. Britton, R. L. Jones, P. I. Oden, Z. Hu, R. J. Warmack, S. F. Smith, W. L. Bryan, and J. M. Rochelle, Ultramicroscopy **82**, 17-21 (2000).
[105]Y. T. Yang, K. L. Ekinci, X. M. H. Huang, L. M. Schiavone, M. L. Roukes, C. A. Zorman, and M. Mehregany, Appl. Phys. Lett. **78**, 162-164 (2001).
[106]S. M. Tabakman, L. Lau, J. T. Robinson, J. Price, S. P. Sherlock, H. Wang, B. Zhang, Z. Chen, S. Tangsombatvisit, and J. A. Jarrell, Nat. Commun. **2**, 466 (2011).
[107]J. N. Anker, W. P. Hall, O. Lyandres, N. C. Shah, J. Zhao, and R. P. Van Duyne, Nat. Mater. **7**, 442-453 (2008).
[108]C. R. Tellier and T. G. Leblois, Sens. Actuators A: Phys. **132**, 224-235 (2006).
[109]P. A. Rasmussen, J. Thaysen, O. Hansen, S. C. Eriksen, and A. Boisen, Ultramicroscopy **97**, 371-376 (2003).
[110]C. H. Wu, C. A. Zorman, and M. Mehregany, IEEE Sensors J. **6**, 316-324 (2006).
[111]L. Jiang, R. Cheung, J. Hedley, M. Hassan, A. J. Harris, J. S. Burdess, M. Mehregany, and C. A. Zorman, Sens. Actuators A: Phys. **128**, 376-386 (2006).
[112]G. Meyer and N. M. Amer, Appl. Phys. Lett. **53**, 1045-1047 (1988).
[113]E. Forsen, G. Abadal, S. Ghatnekar-Nilsson, J. Teva, J. Verd, R. Sandberg, W. Svendsen, F. Perez-Murano, J. Esteve, and E. Figueras, Appl. Phys. Lett. **87**, 043507 (2005).
[114]S. Ghatnekar-Nilsson, E. Forsen, G. Abadal, J. Verd, F. Campabadal, F. Perez-Murano, J. Esteve, N. Barniol, A. Boisen, and L. Montelius, Nanotech. **16**, 98 (2004).
[115]A. R. Kermany, J. S. Bennett, G. A. Brawley, W. P. Bowen, and F. Iacopi, J. Appl. Phys. **119**, 055304 (2016).
[116]M. Mehregany and C. A. Zorman, Thin Solid Films **355**, 518-524 (1999).
[117]A. R. Kermany and F. Iacopi, J. Appl. Phys. **118**, 155304 (2015).
[118]L. Chen, X. Yu, and D. Wang, Ultramicroscopy **107**, 275-280 (2007).
[119]O. Kuter-Arnebeck, A. Labuda, S. Joshi, K. Das, and S. Vengallatore, J. Microelectromech. Syst. **23**, 592-599 (2014).
[120]K. Y. Yasumura, T. D. Stowe, E. M. Chow, T. Pfafman, T. W. Kenny, B. C. Stipe, and D. Rugar, J. Microelectromech. Syst **9**, 117-125 (2000).
[121]R. Sandberg, K. Mølhave, A. Boisen, and W. Svendsen, J. Micromech. Microeng. **15**, 2249 (2005).
[122]F. R. Blom, S. Bouwstra, M. Elwenspoek, and J. H. J. Fluitman, J. Vac. Sci. Technol., B **10**, 19-26 (1992).
[123]H. Hosaka, K. Itao, and S. Kuroda, Sens. Actuators A: Phys. **49**, 87-95 (1995).
[124]R. Lifshitz and M. L. Roukes, Phys. Rev. B: Condens. Matter **61**, 5600 (2000).
[125]A. A. Kiselev and G. J. Iafrate, Phys. Rev. B: Condens. Matter **77**, 205436 (2008).
[126]D. Choi, H. Kim, and W. D. Nix, J. Microelectromech. Syst. **13**, 230-237 (2004).
[127]G. Sosale, S. Prabhakar, L. G. Fréchette, and S. Vengallatore, J. Microelectromech. Syst. **20**, 764-773 (2011).
[128]B. Stipe, H. Mamin, T. Stowe, T. Kenny, and D. Rugar, Phys. Rev. Lett. **87**, 096801 (2001).
[129]S. Ghaffari, S. A. Chandorkar, S. Wang, E. J. Ng, C. H. Ahn, V. Hong, Y. Yang, and T. W. Kenny, Sci. Rep. **3**, 3244 (2013).
[130]M. I. Younis, MEMS Linear and Nonlinear Statics and Dynamics; (Springer, 2011), chap. 4.
[131]C. A. Van Eysden and J. E. Sader, J. Appl. Phys. **101**, 044908 (2007).
[132]M. K. Ghatkesar, T. Braun, V. Barwich, J.-P. Ramseyer, C. Gerber, M. Hegner, and H. P. Lang, Appl. Phys. Lett. **92**, 043106 (2008).
[133]C. A. Van Eysden and J. E. Sader, J. Appl. Phys. **100**, 114916 (2006).
[134]A. Mehta, S. Cherian, D. Hedden, and T. Thundat, Appl. Phys. Lett. **78**, 1637-1639 (2001).
[135]P. Enoksson, G. Stemme, and E. Stemme, Sens. Actuators A: Phys. **47**, 327-331 (1995).
[136]M. Khan, S. Schmid, P. E. Larsen, Z. J. Davis, W. Yan, E. H. Stenby, and A. Boisen, Sens. Actuators B: Chem. **185**, 456-461 (2013).
[137]J. E. Sader, T. P. Burg, and S. R. Manalis, Journal of Fluid Mechanics **650**, 215-250 (2010).
[138]A. K. Pandey, R. Pratap, and F. S. Chau, Exp. Mech. **48**, 91-106 (2008).
[139]S. Schmid and C. Hierold, J. Appl. Phys. **104**, 093516 (2008).
[140]R. A. Barton, B. Ilic, S. S. Verbridge, B. R. Cipriany, J. M. Parpia, and H. G. Craighead, Nano Lett. **10**, 2058-2063 (2010).
[141]M. Imboden and P. Mohanty, Phys. Rep. **534**, 89-146 (2014).
[142]B. Chouvion, S. McWilliam, A. A. Popov, and C. H. J. Fox, Proc. Inst. Mech. Eng. C J. Mech. **226**, 283-295 (2012).
[143]Y. Jimbo and K. Itao, J. Horolog. Inst. Jpn. **47**, 1-15 (1968).
[144]M. C. Cross and R. Lifshitz, Phys. Rev. B: Condens. Matter **64**, 085324 (2001).
[145]D. M. Photiadis and J. A. Judge, Appl. Phys. Lett. **85**, 482-484 (2004).
[146]S. W. Yoon, S. Lee, N. C. Perkins, and K. Najafi, J. Micromech. Microeng. **21**, 015017 (2010).

Copyright line will be provided by the publisher

[147]B. P. Harrington and R. Abdolvand, J. Micromech. Microeng. **21**, 085021 (2011).
[148]K. Wang, A. C. Wong, and C. C. Nguyen, J. Microelectromech. Syst. **9**, 347-360 (2000).
[149]S. Mohammadi and A. Adibi, J. Microelectromech. Syst. **21**, 379-384 (2012).
[150]Y. Tsaturyan, A. Barg, A. Simonsen, L. G. Villanueva, S. Schmid, A. Schliesser, and E. S. Polzik, Opt. Express **22**, 6810-6821 (2014).
[151]L. G. Villanueva and S. Schmid, Phys. Rev. Lett. **113**, 227201 (2014).
[152]J. Yang, T. Ono, and M. Esashi, Microelectromechanical Systems, Journal of **11**, 775-783 (2002).
[153]G. Sosale, D. Almecija, K. Das, and S. Vengallatore, Nanotech. **23**, 155701 (2012).
[154]A. G. Smagin, Cryogenics **15**, 483-485 (1975).
[155]X. Liu, E. Thompson, B. E. White Jr, and R. O. Pohl, Phys. Rev. B: Condens. Matter **59**, 11767 (1999).
[156]G. Fantozzi, Mater. Sci. Forum **366-368**, 3-31 (2001).
[157]S. Prabhakar and S. Vengallatore, J. Microelectromech. Syst. **17**, 494-502 (2008).
[158]L. Sekaric, D. W. Carr, S. Evoy, J. M. Parpia, and H. G. Craighead, Sens. Actuators A: Phys. **101**, 215-219 (2002).
[159]P. S. Waggoner, C. P. Tan, and H. G. Craighead, J. Appl. Phys. **107**, 114505-114505-114505 (2010).
[160]P. L. Yu, T. P. Purdy, and C. A. Regal, Phys. Rev. Lett. **108**, 083603 (2012).
[161]G. Sosale, K. Das, L. Fréchette, and S. Vengallatore, J. Micromech. Microeng. **21**, 105010 (2011).
[162]S. Lee, V. P. Adiga, R. A. Barton, A. M. van der Zande, G. H. Lee, B. R. Ilic, A. Gondarenko, J. M. Parpia, H. G. Craighead, and J. Hone, Nano Lett. **13**, 4275-4279 (2013).
[163]B. V. Cunning, M. Ahmed, N. Mishra, A. R. Kermany, B. Wood, and F. Iacopi, Nanotech. **25**, 325301 (2014).
[164]F. Iacopi, N. Mishra, B. V. Cunning, D. Goding, S. Dimitrijev, R. E. Brock, R. H. Dauskardt, B. Wood, and J. Boeckl, J. Mater. Res. **30**, 609-616 (2015).
[165]M. Ahmed, M. Khawaja, M. Notarianni, B. Wang, D. Goding, B. Gupta, J. J. Boeckl, A. Takshi, N. Motta, and S. E. Saddow, Nanotech. **26**, 434005 (2015).
[166]Y. J. Chang, J. M. Gray, A. Imtiaz, D. Seghete, T. M. Wallis, S. M. George, P. Kabos, C. T. Rogers, and V. M. Bright, Sens. Actuators A: Phys. **154**, 229-237 (2009).
[167]S. S. Verbridge, D. F. Shapiro, H. G. Craighead, and J. M. Parpia, Nano Lett. **7**, 1728-1735 (2007).
[168]H. Ashiba, R. Kometani, S. Warisawa, and S. Ishihara, J. Vac. Sci. Technol., B **30**, 06FD03 (2012).
[169]G. Cagnoli, J. Hough, D. DeBra, M. Fejer, E. Gustafson, S. Rowan, and V. Mitrofanov, Phys. Lett. A **272**, 39-45 (2000).
[170]R. Anzalone, M. Camarda, A. Canino, N. Piluso, F. La Via, and G. D'Arrigo, Electrochem. Solid-State Lett. **14**, H161-H162 (2011).
[171]B. Hähnlein, M. Stubenrauch, S. Michael, and J. Pezoldt, Mater. Sci. Forum **778**, 444-448 (2014).
[172]B. Hähnlein, M. Stubenrauch, and J. Pezoldt, Mater. Sci. Forum **821**, 281-284 (2015).
[173]B. Van Drieënhuizen, J. Goosen, P. French, and R. Wolffenbuttel, Sens. Actuators A: Phys. **37**, 756-765 (1993).
[174]Y. Bellouard, Mater. Sci. Eng., A **481**, 582-589 (2008).
[175]Y. Fu, H. Du, W. Huang, S. Zhang, and M. Hu, Sens. Actuators A: Phys. **112**, 395-408 (2004).
[176]J. K. Luo, R. Huang, J. H. He, Y. Q. Fu, A. J. Flewitt, S. M. Spearing, N. A. Fleck, and W. I. Milne, Sens. Actuators A: Phys. **132**, 346-353 (2006).
[177]J. Gill, D. T. Chang, L. A. Momoda, and G. P. Carman, Sens. Actuators A: Phys. **93**, 148-156 (2001).
[178]P. Schmid, F. J. Hernandez-Guillen, and E. Kohn, Diamond Relat. Mater. **12**, 418-421 (2003).
[179]R. T. Chen, H. Nguyen, and M. C. Wu, IEEE Photon. Technol. Lett. **11**, 1396-1398 (1999).
[180]F. J. Hernandez-Guillen, K. Janischowsky, J. Kusterer, W. Ebert, and E. Kohn, Diamond Relat. Mater. **14**, 411-415 (2005).
[181]J. Pezoldt, T. Stauden, F. Niebelschütz, M. A. Alsioufy, R. Nader, and P. M. Masri, Mater. Sci. Forum **645-648**, 159-162 (2010).
[182]M. A. Matin, K. Ozaki, D. Akai, K. Sawada, and M. Ishida, Comput. Mater. Sci. **85**, 253-258 (2014).
[183]P. Kurzawski, C. Hagleitner, and A. Hierlemann, Anal. Chem. **78**, 6910-6920 (2006).
[184]J. Pei, F. Tian, and T. Thundat, Anal. Chem. **76**, 292-297 (2004).
[185]X. Yan, H. F. Ji, and Y. Lvov, Chem. Phys. Lett. **396**, 34-37 (2004).
[186]G. A. Campbell and R. Mutharasan, Biosens. Bioelectron. **21**, 462-473 (2005).
[187]B. Ilic, Y. Yang, and H. G. Craighead, Appl. Phys. Lett. **85**, 2604-2606 (2004).
[188]D. Yi, A. Greve, J. H. Hales, L. R. Senesac, Z. J. Davis, D. M. Nicholson, A. Boisen, and T. Thundat, Appl. Phys. Lett. **93**, 154102 (2008).
[189]A. Greve, J. Olsen, N. Privorotskaya, L. Senesac, T. Thundat, W. P. King, and A. Boisen, Microelectron. Eng. **87**, 696-698 (2010).
[190]V. T. Srikar and S. M. Spearing, Exp. Mech. **43**, 238-247 (2003).
[191]G. Müller, G. Krötz, and J. Schalk, Phys. Stat. Sol. (a) **185**, 1-14 (2001).
[192]R. Yakimova, R. M. Petoral Jr, G. R. Yazdi, C. Vahlberg, A. L. Spetz, and K. Uvdal, J. Phys. D: Appl. Phys. **40**, 6435 (2007).
[193]O. Cooper, B. Wang, C. Brown, J. Tiralongo, and F. Iacopi, IEEE Access **4**, 477 - 497 (2016).

Copyright line will be provided by the publisher